Available online at www.sciencedirect.com

ScienceDirect

Geochimica et Cosmochimica Acta 221 (2018) 237–254

Geochimica et Cosmochimica Acta

www.elsevier.com/locate/gca

Origin of nanodiamonds from Allende constrained by statistical analysis of C isotopes from small clusters of acid residue by NanoSIMS

Josiah B. Lewis *, Christine Floss, Frank Gyngard

Laboratory for Space Sciences, Physics Department, Washington University, St. Louis, MO, USA

Received 2 October 2016; accepted in revised form 3 June 2017; available online 29 June 2017

Abstract

Meteoritic nanodiamonds carry noble gases with anomalies in their stable isotopes that have drawn attention to their potentially presolar origin. Measurements of $^{12}C/^{13}C$ isotope ratios of presolar nanodiamonds are essential to understanding their origins, but bulk studies do not show notable deviations from the solar system $^{12}C/^{13}C$ ratio.

We implemented a technique using secondary ion mass spectrometry with maximized spatial resolution to measure carbon isotopes in the smallest clusters of nanodiamonds possible. We measured C and Si from clusters containing as few as 1000 nanodiamonds, the smallest clusters of nanodiamonds measured to date by traditional mass spectrometry. This allowed us to investigate many possible complex compositions of the nanodiamonds, both through direct methods and statistical analysis of the distributions of observed isotopic ratios.

Analysis of the breadth of distributions of carbon isotopic ratios for a number of ~1000-nanodiamond aggregates indicates that the $^{12}C/^{13}C$ ratio may be drawn from multiple Gaussian distributions about different isotopic ratios, which implies the presence of presolar material. The mean isotopic ratio is consistent with the solar system value, so presolar components are required to be either low in concentration, or to have a mean ratio close to that of the solar system. Supernovae are likely candidates for the source of such a presolar component, although asymptotic giant branch stars are not excluded.

A few aggregates show deviations from the mean $^{12}C/^{13}C$ ratio large enough to be borderline detections of enrichments in ^{13}C. These could be caused by the presence of a small population of nanodiamonds formed from sources that produce extremely ^{13}C-rich material, such as J-stars, novae, born-again asymptotic giant branch stars, or supernovae. Of these possible sources, only supernovae would account for the anomalous noble gases carried in the nanodiamonds.

Keywords: Nanodiamonds; Presolar grains; NanoSIMS; Isotopes; $^{12}C/^{13}C$

1. INTRODUCTION

Potentially presolar nanodiamonds were first observed in nature in 1987 (Lewis et al., 1987), identified by transmission electron microscopy (TEM) examination of the residual material after acid dissolution, and size and density separations of material from the primitive carbonaceous chondrite Allende. They are ubiquitous in carbonaceous chondrites, at levels up to 1400 ppm by mass (Zinner, 2014). They have a log-normal size distribution that varies from 2.6–3.0 nm in median diameter depending on meteorite and separation method (Lewis et al., 1989; Daulton et al., 1996).

The isolation of these nanodiamonds and their designation as the first type of presolar grain was the result of

* Corresponding author.
E-mail addresses: jblewis@go.wustl.edu (J.B. Lewis), floss@wustl.edu (C. Floss), fgyngard@wustl.edu (F. Gyngard).

http://dx.doi.org/10.1016/j.gca.2017.06.008
0016-7037/

tracing the anomalous Xe isotopic component, Xe-HL, through a series of chemical and physical separation processes. The resulting acid residues contain a number of isotopic anomalies in gases that can be observed by stepped heating. Xe-H has an overabundance of the heavy, *r*-process isotopes ^{134}Xe and ^{136}Xe; Xe-L is enriched in the lighter, *p*-process isotopes ^{124}Xe and ^{126}Xe, relative to solar abundances. As these two nucleosynthetic processes are only known to occur together during supernova explosions, the isotopically anomalous Xe-HL is strong evidence of supernova material present in the acid residues. And, as expected if the nanodiamonds formed from supernova remnant material, there are other isotopically anomalous components present, including excess ^{128}Te and ^{130}Te (Richter et al., 1998), and ^{110}Pa (Maas et al., 2001). No competing mechanism has been proposed to produce Xe-HL other than supernovae. For the nanodiamonds themselves, carbon stars and their environs are obvious source candidates, because they have the required high C/O ratio necessary for C-rich minerals to condense under equilibrium conditions. Lewis et al. (1987, 1989) first suggested that nanodiamonds formed in red giants or planetary nebulae by a mechanism akin to laboratory chemical vapor deposition (CVD), and were later implanted with Xe-HL traveling at 10^3 km/s, presumably provided by the explosion of the host star as a Type II (core-collapse) supernova. Alternatively, it is possible that the nanodiamonds formed in expanding Type II supernova remnants, where chemical and isotopic heterogeneity is expected (Clayton, 1989; Nuth and Allen, 1992; Clayton et al., 1995), or in the envelopes of carbon stars in binary systems, where the companion star later exploded as a Type I supernova, implanting the nanodiamonds with Xe-HL. Notable anomalies in the ^{12}C/^{13}C isotopic ratio of presolar nanodiamonds are expected in any of these scenarios. Finally, it has been suggested that nanodiamonds are formed by supernova shock in the interstellar medium (ISM) (Tielens, 1990; Stroud et al., 2011). Nanodiamonds also carry He, Ne, Ar, and Kr whose isotopic ratios are distinct from solar and appear to be associated with the Xe-HL; as few as 1 in 10^6 grains are required to carry Xe-HL, but to account for these additional trace elements would require roughly 1 in 10 nanodiamonds (Huss and Lewis, 1994a, 1994b, 1995; Huss et al., 2008; see Huss, 2005 for an overview).

The isotopic ratio of ^{12}C/^{13}C (and, to a lesser degree, that of ^{14}N/^{15}N), is the only attribute of these grains that can conclusively establish where the presolar carriers of the Xe-HL formed, since the noble gases may not have co-originated with the grains. Swart et al. (1983) and Russell et al. (1991, 1996) conducted stepped heating measurements on aggregates of billions of nanodiamonds, but found carbon and nitrogen isotopic ratios consistent with solar composition. Small isotopic anomalies, or small fractions of nanodiamonds with larger anomalies, could easily be hidden in these bulk measurements. Thus, there remains debate as to where meteoritic nanodiamonds formed, and whether all the nanodiamonds, or even a majority of them, are presolar (Dai et al., 2002).

The surfaces of the nanodiamonds appear to be damaged by the hydrofluoric and hydrochloric acid treatment, as the infrared spectrum of the acid residue shows absorption from —CH, —COOH, and C—O bonds (Lewis et al., 1989). It is possible, based on infrared spectral observations of the ISM, that the nanodiamonds were originally encased in sp^2-bonded fullerene shells, which were damaged and transformed into disordered C, possibly by the acid dissolution process (Yastrebov and Smith, 2009).

While the acid residue is generally identified as nanodiamond, a significant fraction of it is composed of sp^2-bonded, disordered C. Swart et al. (1983), Russell et al. (1991), and Verchovsky et al. (1998) each note a fraction of material in the residue that releases carbon at lower temperatures and with a ~10 per mil smaller δ^{13}C than that observed for the sample as a whole.

Russell et al. (1991, 1996) conducted stepped heating analyses on nanodiamond residues from a suite of meteorites. The maximum anomalies detected in a single temperature fraction ranged from $\delta^{13}C = -38.8 \pm <0.1$‰ in ALH 83100 (CM2) to $\delta^{13}C = -32.5 \pm 0.1$‰ in Inman (L3.4), relative to Pee Dee Belemnite (PDB, $^{12}C/^{13}C = 88.99$). Our study used Allende (CV3), for which Russell et al. (1991, 1996) obtained a maximum carbon isotopic anomaly of $\delta^{13}C = -35.5 \pm < 0.1$‰. In earlier work Swart et al. (1983) measured a maximum anomaly of $\delta^{13}C = -38$‰ for the as-yet unidentified nanodiamond separate in Allende. Including carbon released at lower temperatures, probably from non-diamond material in the residues, the Allende nanodiamond-containing acid residue has a δ^{13}C value of −30.4‰ (Swart et al., 1983) or -32.7 ± 0.1‰ compared to a range of -28.0 ± 4.4‰ to -36.1 ± 0.1‰ for a variety of other meteorites (Russell et al., 1996). Different separation and analysis techniques are used by different researchers, potentially influencing the results. To summarize these studies, the most anomalous ^{12}C/^{13}C ratio measured in the acid residues is isotopically light, but the magnitude of the anomaly is small compared to the variations found in the solar system.

Implantation is not a viable explanation for the presence of N, as it is for the trace noble gases, so it must have co-originated in the nanodiamonds (Russell et al., 1996). Nitrogen is present in the acid residues at levels ranging from 1800 to 13,000 ppm. The nitrogen is isotopically light compared to nitrogen in terrestrial air, with $\delta^{15}N = -348 \pm 7$‰ (Russell et al., 1996, and references therein), but it is close to the solar value of -383 ± 8‰ determined from Genesis solar wind data (Marty et al., 2011).

Modeling based on Electron Energy Loss Spectroscopy (EELS) data by Bernatowicz et al. (1990) indicates that roughly half the carbonaceous material is disordered. Scanning transmission electron microscopy (STEM) confirmed the presence of disordered carbon and minor elements (Stroud et al., 2011, 2016). It is not clear whether the disordered carbon was a precursor for the nanodiamonds, co-originated with nanodiamonds in the ISM (Stroud et al., 2011), was created by acid dissolution damage of nanodiamonds, or has a different origin from the nanodiamonds and is aggregated from the meteoritic material during the dissolution process. With our methodology (Section 2.2), we cannot easily distinguish between disordered C and nanodiamonds.

In addition to the nanodiamonds and disordered C, the acid residue has been reported to contain ~600 ppm SiC (Lewis et al., 1989), as well as TiC and metal nuggets (Stroud et al., 2016), residual Na and NaOH from laboratory contamination, and F and Cl from the acid treatment (Lewis et al., 2016).

Other studies have revealed evidence of subpopulations within the nanodiamond acid residues. The carbon and nitrogen isotopic ratios are not identical within uncertainties when measured in nanodiamond residues from different meteorites. This is surprising, considering that the concentration of Xe-HL in the residues does not vary greatly between these meteorites, and the ratio of Xe-H to Xe-L is identical (Schelhaas et al., 1990). Russell et al. (1996) observed a carbonaceous component with carbon isotopes slightly depleted in ^{13}C, $\delta^{13}C = -25‰$, that released at lower temperatures during stepped heating. They estimated that this component comprises ~20% of the carbonaceous material. Verchovsky et al. (2006) investigated subpopulations of nanodiamonds by differential centrifugation of acid residues, further isolating material that is coarser and less prone to forming colloids. They found isotopically heavy C, isotopically light N, and different noble gas isotopic signatures compared to the original separates. Although SiC could be responsible for these signatures, Verchovsky et al. (2006) argue that the signatures are from asymptotic giant branch (AGB) star-produced nanodiamonds. $\delta^{15}N$ values range from 0 to $<-350‰$ in stepped heating from Allende (Russell et al., 1991), although the initial, relatively ^{15}N-rich signal could be fractionation caused by preferential loss of ^{14}N-rich molecular N_2 in the laboratory. In an ongoing study, nanodiamonds have been separated into subpopulations based on size, degree of chemical surface damage, and fraction of disordered C, using electrophoresis (Shatoff et al., 2015; Stroud et al., 2016; Pravdivtseva et al., 2016).

With the exception of ongoing investigations using atom-probe tomography (Isheim et al., 2013; Heck et al., 2014; Lewis et al., 2015), no viable methods exist for measuring the $^{12}C/^{13}C$ ratio in individual nanodiamonds, due to limitations in size and atomic count. Thirty-four ng of nanodiamond acid residue, the smallest sample we have found reported (Swart et al., 1983, in a single stepped heating step), should contain roughly 10^{15} atoms, enough for 10^{12} nanodiamonds (given a diamond density of 3.51 g/cm^3).

To investigate these potential subpopulations, we measured thousands of clusters of as few nanodiamonds as possible, using nanoscale secondary ion mass spectrometry (NanoSIMS) with a minimized beam spot, collecting data from thousands of small regions across a deposit of nanodiamonds (Sections 2.1 and 2.2). The resulting data are sensitive to a variety of isotopic signatures that, if present, would indicate presolar origins, which may not be evident in larger bulk studies because of dilution and averaging of anomalies (Section 2.3). The data were analyzed to determine the overall $^{12}C/^{13}C$ ratio (Section 3.1), and to search for outlier ratios (Section 3.2) and significant broadening of the distribution of measured ratios (Section 3.3), which would indicate multiple isotopic sources. After discussing silicon observed in the acid residues (Section 3.4), we present detection limits and assess what isotopically anomalous populations are ruled out by our data (Section 3.5). In Section 4, we discuss the implications of the data for existing research and for the probable stellar origins of nanodiamonds, and summarize our conclusions in Section 5.

2. METHODS

2.1. Samples

A droplet of nanodiamond-bearing Allende acid residue, designated DM (Lewis et al., 1989), suspended in deionized water was deposited onto gold foil by Roy Lewis (Fig. 1a).

For standards, we used 4–7 nm diameter nanodiamonds created by detonation (Greiner et al., 1988) that were separated and prepared similarly to the Allende deposit (Fig. 1b). Additional standards included DAG carbon paint, $\delta^{13}C = (-29.3 \text{ to } -24.6) \pm 1.7‰$ relative to PDB (Amari et al., 2014), and a polished graphite planchette (Fig. 1c). We observed much lower count rates for the detonation nanodiamond standards than the Allende nanodiamonds. A possible explanation is that the detonation nanodiamond deposits onto gold foil are much sparser than the meteoritic nanodiamond deposits.

The abbreviations for the samples are ADM (Allende DM nanodiamond-containing acid residue), DND (detonation nanodiamond acid residue standard), GRP (polished graphite planchette), and CPT (DAG carbon paint).

2.2. Data collection

Our experimental goal was to conduct thousands of measurements of ^{12}C and ^{13}C, each of as few nanodiamonds as possible. We used the Cameca NanoSIMS 50 at Washington University in St. Louis. We chose this instrument for its high spatial resolution (down to 50 nm), mass resolving power sufficient to distinguish ^{13}C from $^{12}C^1H$, and multicollection that allowed us to simultaneously collect ^{12}C and ^{13}C for the major isotope ratio and ^{28}Si to detect SiC or any other Si-bearing phase in the acid residue. Using the NanoSIMS, we bombarded the sample with a Cs^+ primary beam, implanting Cs ions and sputtering away material. The NanoSIMS achieves a small primary beam spot, and thus high spatial resolution, through the use of co-axial primary and secondary ion beams, which allows the ion extraction optics to be placed much closer to the sample than in other SIMS instruments, and by using a primary beam that is perpendicular to the sample, minimizing the cross section of the sample struck by the beam. In order to measure as few nanodiamonds as possible in aggregate, we tuned the NanoSIMS to a small beam. While the beam size has numerous dependencies, the key changes we made were using a source demagnification lens to decrease the primary beam size and using the smallest field aperture diaphragm in the immersion lens. The secondary ion current is low, not only because of the smaller primary beam diameter, but also due to a drop in current density inherent to this configuration.

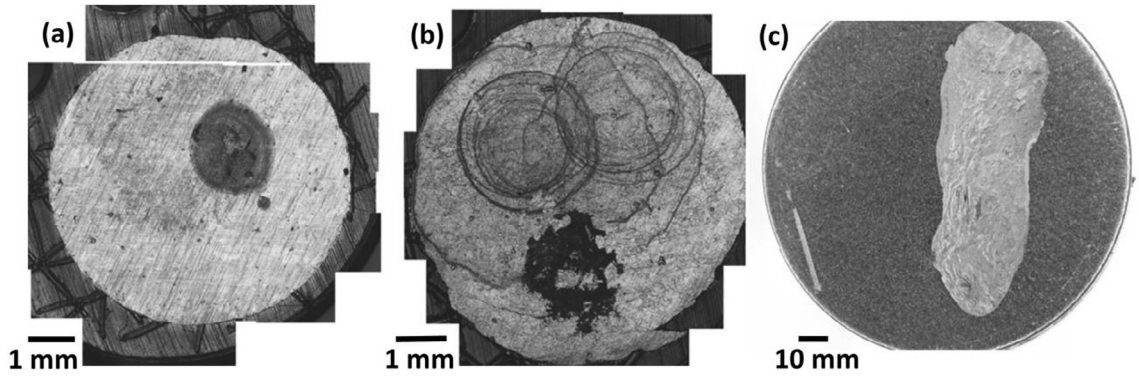

Fig. 1. Grayscale mosaics of reflected light optical microscopy images of samples. (a) Stub with Allende DM nanodiamond residue on gold foil. (b) Stub with terrestrial detonation nanodiamonds on gold foil. (c) Stub made of polished graphite (darker). "DAG" carbon paint (lighter) was applied to the right-hand side.

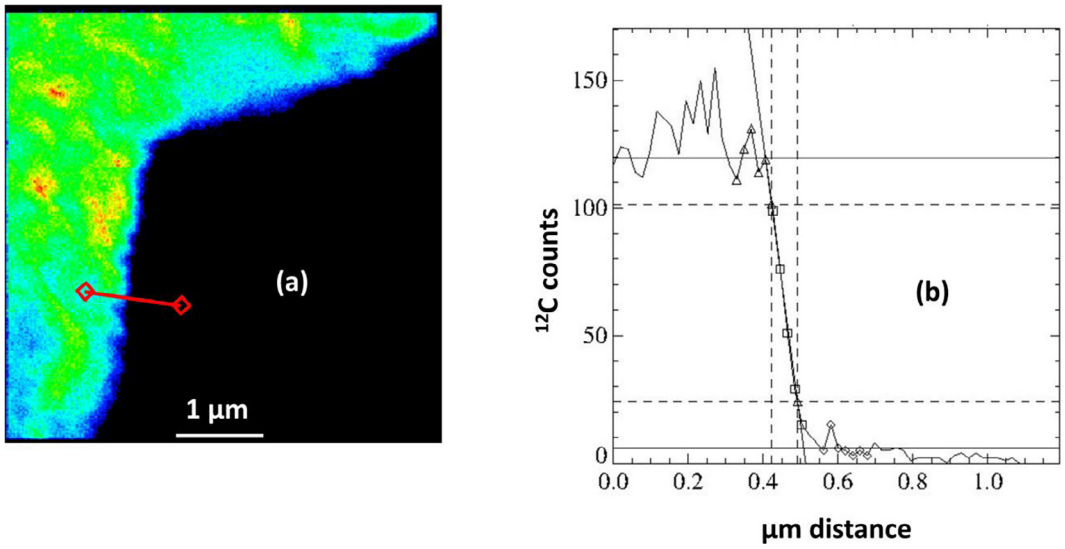

Fig. 2. Beam diameter minimization. We conducted a linescan across a near-step function in signal intensity (a), represented by the red line and diamond endpoints. The beam full width half max is given by fitting the linescan data (b), where boxes denote points used to fit the signal drop-off, and triangles and diamonds denote points used to fit the high and low signals, respectively. The width of the beam is taken to be the distance over which the beam falls from 84% to 16% intensity, and in this case is less than 70 nm. (For interpretation of the references to colour in this figure legend, the reader is referred to the web version of this article.)

To measure the primary beam diameter, we scanned the beam perpendicularly across a sharp boundary between carbon paint and a void (Fig. 2a). For our small beam, the signal should fall off rapidly, based on the width of the material transition (close to a step function) convoluted with the size of the beam. We measured the signal on either side of the boundary and calculated how far the beam traverses as the signal intensity falls from 84% to 16%, resulting in an upper limit for the beam size. Over a number of measurements, the smallest this value fell to was 70 nm (Fig. 2b). We emphasize that this is an upper limit; we expect our beam was closer to 50 nm in size, but so as not to dramatically overestimate our sensitivity to isotopic anomalies, we take 70 nm as our beam diameter. Spot sizes as small as 30 nm in diameter have been reported for the NanoSIMS (e.g., Hoppe et al., 2015). Such measurements would reduce the number of nanodiamonds analyzed per beam spot by 80% (such a change would be an improvement but not an unqualified one, the accompanying drop in counts as a result of measuring less material would slow data collection).

To serialize acquisition of spot measurements, we used imaging mode with an image size of $1.2 \times 1.2\ \mu m^2$ and 16×16 pixels, where the distance between two pixels (75 nm) is larger than the beam full width half max, minimizing overlap in the material measured. We used multiple cycles with the maximum dwell time of 1 s. The time between each 1 s dwell on a spot is 256 s. It took several hours to acquire 256 pixel data sets with 26–150 cycles. Table 1 gives the number of cycles, carbon count rates, and collection time for each data set. If the primary beam experienced extreme drift, on the order of 50 nm during

Table 1
Measurement conditions for each NanoSIMS data set.

Data set[a]	Cycles	Mean C counts per pixel per cycle	Analysis time (minutes)
ADM 26-1	60	1130	256
ADM 26-3	130	279	555
ADM 27-3	122	180	521
DND 25-4	105	28	448
DND 28-1	60	64	256
DND 28-3	35	91	149
GRP 29-2	26	3020	111
GRP 29-4	150	3123	640
CPT 28-1	91	2279	388

[a] ADM: Allende DM nanodiamond-containing acid residue. DND: Terrestrial detonation nanodiamond-containing acid residue. CPT: Carbon paint. GRP: Graphite planchette.

the time between the first and last 1 s dwell on a pixel, it would as much as double the number of nanodiamonds sampled for that pixel, decreasing our sensitivity to anomalies in small areas. Unfortunately, the analysis software did not allow us to use longer dwell times in imaging mode, and to conduct thousands of measurements in spot mode would have been prohibitively time intensive. It would be ideal if the control software allowed for the automated collection of large numbers of depth profile measurements, as this would minimize drift time per pixel. However, drift correction algorithms in the L'Image image processing software suggest the drift is already smaller than one 75 nm diameter pixel.

In order to assess our sensitivity to isotopic anomalies, it is important that we know how much material we have analyzed. Making such an estimate is non-trivial. One method for approximating the number of nanodiamonds sampled from (N_C) is based on the number of carbon counts detected, n_D:

$$N_C = \frac{n_D}{\frac{4}{3}\pi r^3 \rho_D U} \quad (1)$$

where r is the radius of a spherical unit of Allende nanodiamond-containing acid residue, ρ_D is the number of carbon atoms per volume of diamond, 176 carbon atoms per nm^3, and U is the useful yield. This method does not require knowledge of the size of the crater excavated, but also does not take into account nanodiamonds that were only partially milled. Further, by incorporating the expression for the number of carbon atoms per nanodiamond, Eq. (1) uses the assumption that units of disordered carbon have the same number of carbon atoms as nanodiamonds, that is, Eq. (1) assumes that units of disordered carbon have the same mass, rather than the same volume, as the nanodiamonds. Another method for approximating the number of nanodiamonds from which we sampled is based on the volume of material sputtered through:

$$N_V = \frac{R^2 d}{\frac{4}{3} r^3} \quad (2)$$

where R is the radius of the Cs^+ primary beam, and d is the depth to which the sample was milled.

For both estimates, it is important to define the radial unit size of the carbonaceous material analyzed, r. The unit size for the disordered carbon is unknown, while that of the nanodiamonds is a log-normal distribution (Lewis et al., 1987; Daulton et al., 1996) covering several orders of magnitude in volume, with a median value of 2.7 nm in diameter for Allende DM. The sp^2-bonded disordered carbon has undergone the same separation procedures, so we expect a single unit of this material to be similar to the nanodiamonds. Eq. (1) includes the approximation that a unit of nanodiamond or disordered carbon will contain the same number of carbon atoms. Eq. (2) uses the different approximation that a unit of nanodiamond or disordered carbon will take up the same volume. The difference between these approximations is the difference between the densities of C atoms in the two phases. The density of disordered carbon is ~1.5 g/cm^3, or ~75 carbon atoms/nm^3 (Shigemitsu et al., 1979) and that of diamond is 3.51 g/cm^3, or 176 carbon atoms per nm^3. We take an intermediate value as the density of the nanodiamond-containing acid residue, $\rho = \sim 2.5$ g/cm^3, that is, ~125 carbon atoms per nm^3. The residue is composed of disordered sp^2-bonded carbon and sp^3-bonded diamond, possibly with layered shells of sp^2-bonded C. It is unclear if there is any void space in between units of disordered carbon and nanodiamonds. It is likely that there is variability in how compact the disordered material is packed and what fraction of the material is diamond.

We define U, the useful yield, as the fraction of carbon atoms sputtered from the sample that are also detected by the NanoSIMS. Only a fraction of sputtered material is ionized, and only a fraction of that ionized material arrives at the detectors. The higher our estimate of U, the higher our estimate of sensitivity to isotopic anomalies will be. We use $U = 0.5\%$ in order to not overestimate our sensitivity. For comparison, we routinely achieve ~1% Si useful yield on a Si wafer, and C yields of at least as high as 3% have been reported for C film (Hillion et al., 1995).

Given these values, we estimate that the typical nanodiamond contains an average of ~2000 atoms, that $N_c = \sim 0.11 \times n_D$, and that we detect approximately 10 atoms per nanodiamond or unit of disordered carbon. We will use "cycle" to refer to the raw data from a 1s NanoSIMS beam shot, and "data point" to refer to the counts summed over multiple consecutive cycles from the same pixel to add up as close as possible to the target count of 2917 $^{12}C + {}^{13}C$

atoms. 2917 is the average number of $^{12}C + ^{13}C$ for a data point summed over all cycles for a pixel in the data set with the lowest count rates, DND 25-4. Data points for other data sets were similarly constructed by summing over a number of cycles until they contain as close as possible to an average 2917 $^{12}C + ^{13}C$ counts. If each nanodiamond and unit of disordered carbon in the beam contains the average number of carbon atoms and is milled completely through, the counts-based estimate for the number of nanodiamonds and units of disordered carbon, Nc, is ~300. However, if we milled through less than 3 nm of material, it would be incorrect to assume we sampled from only N_c nanodiamonds. Instead, we would have sputtered partway through N_V nanodiamonds, where d is 3 nm.

Given the values of r, and the primary beam R, that we have estimated, the number of nanodiamond-sized units of volume sputtered through in a data point is $N_V = 373 \times d$. However, this does not take into account packing or the different densities of the disordered sp^2 carbon and the nanodiamonds, and the assumed geometry requires $d = 3$ nm or greater. For every 3 nm layer, there is enough volume for roughly 1000 nanodiamonds.

The counts and cross-section approximations vary by more than a factor of two, estimating that there are 300 and 1000 nanodiamonds, respectively, per 3 nm layer in a 70 nm diameter spot size. In addition, positively charged 8 kV Cs ions should penetrate significantly farther into a carbonaceous sample than the ~3 nm diameter of a typical nanodiamond (stopping and range of ions in matter simulations give 14 nm; Ziegler et al., 2010), creating some amount of amorphization and mixing. So even if we correctly estimate how much material is sputtered away, we cannot be positive none of the sputtered material was gardened up to the surface from a greater depth. For these reasons, there is uncertainty as to the depth milled, but both counts-based and volume-based methods agree that the 2917 average C count data points sample only from the top layer of nanodiamond-containing acid residue.

To measure d, the depth sputtered through, we excavated a series of cross-sections out of one of the 1.2×1.2 μm^2 analysis areas using a Ga focused ion beam (FIB) microscope and performed secondary electron imaging. Fig. 3 shows one of these cross-sections. At the edge of the sputtered region what appears to be a presputter crater edge is visible, with a depth of 30–60 nm, but no further excavation is visible. A series of 10–20 nm deep craters should be resolvable, but craters less than 3 nm in depth would not be. We also estimated the mill depth using the equation

$$d = \frac{n_D}{\pi R^2 \rho U} \tag{3}$$

which gives the mill depth based on the carbon counts collected, and the estimations of the average density and beam spot size, reducing to $d = (4 \times 10^{-4}) \times n_D$. Summed over all cycles for the Allende data sets, counts per pixel range from $2–7 \times 10^4$ counts, giving d on the order of 10 nm. This is large enough to be resolved by our cross-sections. Using $n_D = 2917$ carbon counts per data point gives an approximate mill depth of 1 nm.

For measurements that sum counts across all cycles in a pixel, we use the counts-based approach to estimate the number of nanodiamonds we have milled through.

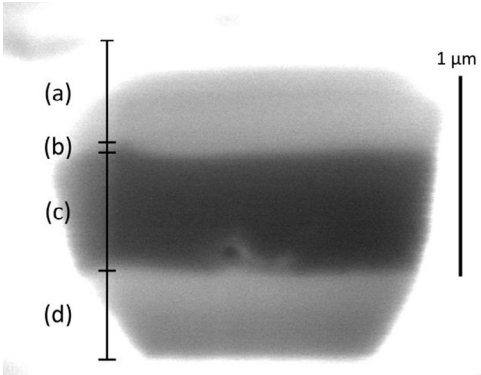

Fig. 3. Cross section of deposit after NanoSIMS analysis. Secondary electron image obtained with a FIB/SEM dual-beam microscope. (a) FIB-deposited Pt layer applied prior to sectioning. (b) Depth of NanoSIMS presputter (30–60 nm). (c) ADM deposit (~600 nm). (d) Gold foil beneath deposit.

2.3. Data reduction

We used custom scripts to read Cameca *.im* binary data files, and to reduce and analyze the data. Images are not drift corrected, because drift corrections use pixel-size steps, while our beam spot is sub-pixel in size. Drift correction algorithms in the L'Image software suggested at most one-pixel shifts. Our instrument has a 36 ns deadtime, which we do not correct, because corrections will be insignificant (less than 1 count for any pixel with fewer than 5270 counts detected), which includes all the pixels in our data. See Table 1 for the average $^{12}C + ^{13}C$ counts per pixel per cycle for each data set. Ratio measurements made under the same experimental conditions on the same or a similar matrix will be equally affected by QSA (Slodzian et al., 2004). All our analyses are either on ratio measurements on the same matrix, or are Allende nanodiamond materials normalized to detonation nanodiamond material, which is a comparable matrix. Thus our results are not affected by the QSA effect, so we did not attempt to correct for it. The uncertainty in a ratio calculation is based on counting statistics for the counts of each isotope collected. Calculations with 0 counts for an isotope of carbon were discarded. To exclude calculations made with counts far lower than the target number, we discarded pixels with 2.5 times less than the maximum $^{12}C + ^{13}C$ counts for a pixel of a data set. Pixels were checked for potential SiC or silica using the ^{28}Si counts as well as the ratio of ^{28}Si counts to summed C counts.

2.3.1. Bulk ratio analysis

We report the ratio as per mil deviation, using the bulk ratio from the 3 DND data sets as our standard:

$$\delta^{13}C_{bulk} = \left(\frac{\left(\frac{^{13}C}{^{12}C}\right)_{ADM}}{\left(\frac{^{13}C}{^{12}C}\right)_{DND}} - 1 \right) * 1000 \tag{4}$$

The uncertainty in the bulk C isotopic anomaly, *Err* ($\delta^{13}C_{bulk}$) is the sum in quadrature of (1) the fractional standard deviation of the $^{13}C/^{12}C$ ratios for the data from each of the three grids, and (2) the fractional standard deviation calculated from three grids of terrestrial detonation nanodiamonds. In per mil this is given by:

$$Err(\delta^{13}C_{bulk}) = 1000\frac{\left(\frac{^{13}C}{^{12}C}\right)_{ADM}}{\left(\frac{^{13}C}{^{12}C}\right)_{DND}} \times \sqrt{\left(\frac{\sigma_{ADM}}{\left(\frac{^{13}C}{^{12}C}\right)_{ADM}}\right)^2 + \left(\frac{\sigma_{DND}}{\left(\frac{^{13}C}{^{12}C}\right)_{DND}}\right)^2}\ ‰ \quad (5)$$

The bulk $^{13}C/^{12}C$ ratio was calculated from 3×10^7 carbon counts from 768 pixel spots located in three $1.2 \times 1.2\ \mu m^2$ grid areas, designated as data sets ADM 26-1, ADM 26-3, and ADM 27-3. We estimate these data represent approximately 8×10^9 carbon atoms sputtered from the sample, taken from 4×10^6 nanodiamonds (or 2×10^6 nanodiamonds and accompanying disordered carbon). While results are reported and discussed in terms of $^{12}C/^{13}C$, analyses were conducted using $^{13}C/^{12}C$, to prevent low counts in the denominator from skewing the calculation of the standard deviation. Bulk $^{13}C/^{12}C$ ratios, prior to standardization, are calculated as the sum of ^{13}C counts from all pixel spots from the three Allende data sets *i*, divided by the sum of ^{12}C counts:

$$\left(\frac{^{13}C}{^{12}C}\right)_{bulk} = \frac{\sum_i {}^{13}C_i}{\sum_i {}^{12}C_i} \quad (6)$$

where for this calculation, $\left(\frac{^{13}C}{^{12}C}\right)_{bulk} = \left(\frac{^{13}C}{^{12}C}\right)_{ADM}$ or $\left(\frac{^{13}C}{^{12}C}\right)_{DND}$. We sum all counts from an isotope prior to dividing, since averaging over a number of calculated ratios, even with proper weighting, introduces a positive bias in the ratio (Ogliore et al., 2011).

For this calculation and others in the manuscript, the weighted standard deviation σ of an isotopic ratio or a number *i* of data points or data sets is defined as

$$\sigma_{\left(\frac{^{13}C}{^{12}C}\right)_{bulk}} = \sqrt{\frac{\Sigma_i w_i}{\left(\Sigma_i w_i\right)^2 - \Sigma_i w_i^2} \sum_i w_i \left(\frac{^{13}C_i}{^{12}C_i} - \left(\frac{^{13}C}{^{12}C}\right)_{bulk}\right)^2}. \quad (7)$$

$\left(\frac{^{13}C}{^{12}C}\right)_{bulk}$ is the ratio for which the standard deviation is being calculated. For σ_{ADM} and σ_{DND}, *i* is the index for the data from one data set of Allende, or detonation nanodiamonds, respectively, but elsewhere in the manuscript *i* represents data from pixels rather than data sets. The weights are defined as

$$w_i = \left(\frac{1}{Err(^{13}C_i/^{12}C_i)}\right)^2 \quad (8)$$

These are the weights for each data point or data set *i*, based on the uncertainty in the $^{13}C/^{12}C$ ratio of the summed isotope counts for each data set. This takes into account the width of the error bars on each data point in terms of $^{13}C/^{12}C$ ratio. For the same $^{12}C + {}^{13}C$ counts in a given data point, ^{13}C-enriched data points have larger ratios and thus larger absolute uncertainties and lower weights, in spite of having lower fractional uncertainties.

Using the methods described above, the terrestrial standard nanodiamonds have a raw, that is, un-normalized $^{12}C/^{13}C$ ratio of 98^{+3}_{-4} over three data sets, designated DND 25-4, DND 28-1, and DND 28-3. While per mil precision isotopic studies of the detonation nanodiamond separates we used are not available, the real value for these nanodiamonds should be close to the known terrestrial value (~89, Coplen et al., 2002); the difference indicates that matrix effects, topography, and potential systematic errors do significantly affect our small-beam measurements on acid residue deposits, and that proper standardization is essential.

2.3.2. Broadening analysis

We searched for indications of isotopic anomalies by examining the shape of distributions of $^{13}C/^{12}C$ ratios for Gaussian broadening compared to the shape expected from statistics and standards. Given sufficiently low variance in the denominator, the quotient of two Gaussian distributions may be modeled as a Gaussian (Hayya et al., 1975). If there is isotopically anomalous material in the acid residues, distributions of ratio measurements will be the combination of multiple distributions. All the data points with counts from isotopically anomalous nanodiamonds may be well within uncertainty of the mean, and the distribution need not be double-peaked, but the distribution will be broader overall if the material is drawn from more than one isotopic reservoir. Systematics can produce Gaussian and non-Gaussian broadening, so we corrected our data using standards.

(1) To calculate the amount of systematic broadening (that is, non-Gaussian broadening), we used the term

$$B_S = \frac{\sigma_{observed} - \bar{\sigma}_{expected}}{\bar{\sigma}_{expected}} \quad (9)$$

$\bar{\sigma}_{expected}$ is the standard deviation (Eq. (7)) of the carbon isotopic ratio derived from the assumption that the data fit a Gaussian distribution.

We fit $\sigma_{observed}$ in our standards using a reduced chi-squared model. The reduced chi-squared for a distribution of $^{13}C/^{12}C$ ratio data points is given by:

$$\chi^2_{red} = \sum_i \left(\frac{^{13}C_i/^{12}C_i - (^{13}C/^{12}C)_{bulk}}{\sigma}\right)^2 \Big/ dof \quad (10)$$

where the mean ratio is the ratio of the summed counts over all data points *i*, *dof* is the number of degrees of freedom, that is, the number of data points, *N*, minus 1, and σ is the fitted parameter. We used $\bar{\sigma}_{expected}$ (Eq. (7)) as the initial value of σ. If the residual $\chi^2_{red}-1 \neq 0$, indicating a non-optimal fit, we adjusted σ by a fraction of the residual and recalculated χ^2_{red}. This process was repeated until $\chi^2{}_{red}$ converged to a value of one. The final value of σ is $\bar{\sigma}_{observed}$.

Given these definitions for $\bar{\sigma}_{observed}$ and $\bar{\sigma} - expected$ we calculated *Bs*. We used all the data points from a given data set in a single distribution, which minimizes the uncertainty.

On the order of 10^6 nanodiamonds are present in each of the three Allende distributions.

(2) To calculate Gaussian broadening we compared directly to the standards. We subtracted the mean fractional deviation of our standard data sets from the fractional standard deviation, σ, for the data set for which we are calculating the Gaussian broadening,

$$B_G = \sigma - \bar{\sigma}_{Standards} \tag{11}$$

where $\bar{\sigma}_{Standards}$ is the average fractional σ for the DND, GRP, and CPT data sets. $Err(B_G)$, the uncertainty in B_G, is the sum in quadrature of $Err(\sigma)$ and $Err(\bar{\sigma}_{standards})$. The uncertainty in the standard deviation is given by,

$$Err(\sigma) = \frac{\sigma}{\sqrt{2(N-1)}} \tag{12}$$

(Taylor, 1997, 294–298), where, for σ_{ADM}, N is the number of data points in the data set being evaluated for Gaussian broadening, and for $\sigma_{standards}$ N is the number of data sets averaged over (in which case N = 6).

Given that we corrected for B_S, the systematic broadening, if B_G exceeds the uncertainty, there are two explanations: Either a statistical difference in the data set is simulating the presence of multiple distributions, or the Allende data set contains isotopically anomalous material.

If the counts per data point vary in a distribution of data points, the effect on the standard deviation will be similar to drawing from multiple different distributions, each with a different number of counts per data point. This will lead to broadening of the distribution compared to one created from data points that each have identical counts. For each data set, we calculated the standard deviation of the ^{12}C counts for all the data points in the data set, and tested if the Gaussian broadening depends on this value. Broadening for data sets that do not fall along a linear correlation fit cannot be attributed to this effect.

2.3.3. Outlier analysis

We continued our search for isotopic anomalies by creating distributions of $^{13}C/^{12}C$ isotope ratio data points to search for outliers. We divided the Allende data into a total of 72,103 data points, each from a single spot summed over cycles to include as close as possible to 2917 carbon counts, which is the mean number of carbon counts-per-pixel (summed over all cycles) for DND 25-4, the data set with the lowest count rates. It is serendipitous that 2917 counts corresponds to roughly 1 nm mill depth, sampling from one, but only one, layer of approximately 1000 nanodiamonds, as this allows us to measure the isotopic ratio from a minimum number of nanodiamonds and still have data points that sample from a similar number of nanodiamonds for each data set and material, in spite of the low counts from the detonation nanodiamond standards.

We used a rolling sum, so each cycle of raw data from a pixel is included in n data points, where n is the number of cycles summed over to achieve the target counts (this is a simplification as n is not always the same for every data point in a sample). For example, given consecutive cycles 1, 2, 3, 4, and 5, and $n = 3$, the first data point will sum cycles 1, 2, and 3 before reaching the target counts; the second data point will start at cycle 2 and sum cycles 2, 3, and 4. Data point three will sum cycles 3, 4, and 5. Data point four starts at cycle four. So cycle 3 is included in n (three) data points. If instead of a rolling sum, we skipped over previously summed cycles we would have up to an $(n-1)/n$ chance to overlook any outlier. In the worst-case scenario, an isotopic anomaly persists over exactly n cycles. For example, suppose the counts from cycles 2–4 in our example are anomalous enough to constitute an outlier. A rolling sum with $n = 3$ will detect an outlier in the second data point, which sums cycles 2–4. But an exclusive sum starting at cycle 1 or cycle 3 will dilute the signal with non-anomalous cycles 1 or 5 and not detect the outlier. Thus, 2/3 of the time, or $(n-1)/n$ of starting points, this outlier would be missed. After the first rolling sum in a pixel sums to the last cycle of the data set, we do not consider data points starting at subsequent cycles, as these will all sum to the end of the data set without reaching the target 2917 C counts, and therefore do not represent any new data.

Each data point represents approximately 8×10^5 carbon atoms sputtered from the sample, or as many as 1000 nanodiamonds (or fewer nanodiamonds and accompanying disordered carbon). By using data points that have close to the same counts on average, we created statistically similar distributions from data sets taken from different sample areas and materials. For the calculation of the standard deviation, each data point was weighted based on the uncertainty due to counting statistics for each of the isotopes. The typical weights, which in this case we will call w' were normalized as w, such that $\Sigma_i w_i = N$, the number of measured ratios, using

$$w_i = N\frac{w_i'}{\Sigma_i w_i'} \tag{13}$$

where

$$w_i' = \left(\frac{1}{Err(^{13}C_i/^{12}C_i)}\right)^2. \tag{14}$$

Using normalized weights allowed us to use the simple, unweighted expression for the fractional uncertainty in the standard deviation (Eq. (12)).

The mean ratio is calculated as the sum of ^{13}C counts divided by the sum of the ^{12}C counts, to avoid the bias that would be introduced by averaging over a number of ratios (Ogliore et al., 2011). The uncertainty in the mean ratio is given by the standard error of the mean, SEOM,

$$SEOM = \frac{\sigma}{\sqrt{N}}. \tag{15}$$

For readability, ratios are plotted in terms of $^{12}C/^{13}C$, but the distributions are displayed linearly with respect to $^{13}C/^{12}C$, to avoid the appearance of tails at high $^{12}C/^{13}C$ ratios, due to low counts in the denominator of $^{12}C/^{13}C$ ratio data points.

To be identified as an isotopic anomaly, data points with 4σ or greater deviation from the bulk isotopic ratio were analyzed further against several more criteria. First, they must have more than half the average relative significance, that is, the average w_i, for data points in the data set. Second, analysis of depth profiles for each signal (^{12}C, ^{13}C, ^{16}O, ^{28}Si, and secondary electrons), as well as for $^{13}C/^{12}C$, must show that the anomaly exists over multiple cycles, with stable counts from the other ions and secondary electrons. Because of lower count rates in ADM compared to CPT and GRP standards, each data point in the ADM data is summed over more cycles to create roughly comparable counting statistics; therefore, an outlier in Allende is much less likely to be attributable to an instrumental artifact, which should affect only a single cycle.

2.3.4. Detection limit calculation

In order to assess which anomalous components our experiment rules out by non-detection, we posited a model of the isotopic composition of the nanodiamonds. We take a simple, two-component model, a normal component with isotopic ratio R_n equal to the solar system value, and an anomalous component, with a ratio, R_a, comprising a fraction, f_a, of a sample, and resulting in an observed ratio R_O. We derived an expression relating f_a and R_a for a given R_O, and R_n. When the number of σ deviations from the bulk ratio that constitutes detection of an outlier is used for R_O, the curve $f_a(R_a)$ denotes the detection limit:

$$f_a(R_a) = \frac{(R_a + 1)(R_o - R_n)}{(R_a - R_n)(R_o + 1)} \quad (16)$$

This expression is for ratios in terms of $^{12}C/^{13}C$. For the sensitivity of the bulk ratio technique described in Section 3.1, we used the measured bulk C isotopic ratio that would constitute a 2σ outlier as R_O. To assess the sensitivity of the outlier ratio technique described in Section 3.2 to individual aggregates that are isotopically anomalous, we calculated the ratio that would constitute a 5σ outlier for a data point in our Allende data, and use that ratio as R_O.

3. RESULTS

3.1. Bulk $^{12}C/^{13}C$ ratio

The "bulk" isotopic composition of the Allende nanodiamonds we measured is $\delta^{13}C = 8 \pm 35‰$, normalized to the detonation nanodiamonds (Fig. 4). The uncertainty includes counting uncertainty, matrix effects, topography, and differences between sample and standard as well as tuning on different data collection runs. We estimate this measurement sputtered through 8×10^9 atoms of Allende acid residue, and represents approximately 4×10^6 nanodiamonds. Our results are consistent with solar system values. There is a small enrichment in ^{13}C in our samples compared to previous studies, at the 1σ level.

3.2. Outlier ratios

Distributions of $^{12}C/^{13}C$ isotopic ratio measurements for each data set are plotted in Fig. 5. Since the measurements on Allende were from three different 1.2×1.2 μm^2 areas on the sample, we plotted three different distributions. Fig. 5 also includes the distributions from the terrestrial detonation nanodiamonds, graphite, and carbon paint standards. ADM 27-3 is distinct from the other two Allende data sets in that it does not have tails of the same length, nor is the peak as smooth of a curve. It also has the highest mean $^{12}C/^{13}C$ ratio and standard deviation. Table 2 describes the mean, standard deviation, and uncertainties for these isotopic ratio distributions, using $^{13}C/^{12}C$ since the standard deviation, uncertainty in the standard deviation, and uncertainty in the mean are all asymmetric in $^{12}C/^{13}C$. The standard deviation should be similar for each data set, because the counts per data point are similar values as a result of summing over multiple cycles to a target count. Even though different data sets contain dramatically different numbers of data points, each data point has similar uncertainty, and, therefore, contributes to a similar distribution, so long as systematic errors are minimal, and each distribution is drawn from only one mean ratio.

The Allende data contain 5 data points that are over 4σ away from the mean ratio for their respective data sets (Table 3, Fig. 6), 3 from ADM 26-1 and 2 from ADM 26-3. The two outlier data points in ADM 26-3 are from consecutive sets of summed cycles in the same pixel (located at row 13, column 4), and therefore share most of the same raw data cycles. The three outlier data points in ADM 26-1 are not from physically adjacent pixels in the analysis. None of the Allende outliers included the first cycle of a data set. All are ^{13}C-rich; after normalizing to the detonation nanodiamond standards, they have $\delta^{13}C$ on the order of 800‰, near $^{12}C/^{13}C = 50$. Across these three data sets, we predict we would see 4 or 5 outliers $>4\sigma$ given a Gaussian distribution and the same significance for every data point (Table 4). The detonation nanodiamond standards are not instructive in comparison since the expected and observed frequency of 4σ outliers are both less than one. In the graphite data we expect 3 or 2 $>4\sigma$ outliers and observed 3, the most extreme of which was 4.7σ away from normal. In the carbon paint we expect 1 or 2 outliers $>4\sigma$ and observed 4, although one was in the first cycle of the data set, which is prone to artifacts. The outliers in our standards demonstrate that systematics in our analytical approach can produce outliers larger than those observed in our measurements of Allende, and at similar frequency per data point, possibly due to background spikes or electronics artifacts. However, a key difference between the standard and Allende data is that depth profiles show that the anomalous data points in Allende are consistent over several cycles, whereas all 7 outliers from the standards are the result of increased counts in only a single cycle (Fig. 7). In each case, the outlier is a peak in a curve composed of 2–5 ^{13}C-rich data points, each of which is summed over multiple raw data cycles, collected minutes or hours apart, and thus not attributable to background or artifacts. 3 data points represent ~3 nm in depth milled based on our approximations – that is, the diameter of the average Allende nanodiamond. For the standards GRP and CPT, each outlier is only one data point deep, and in each case the data point is only composed of data from one cycle.

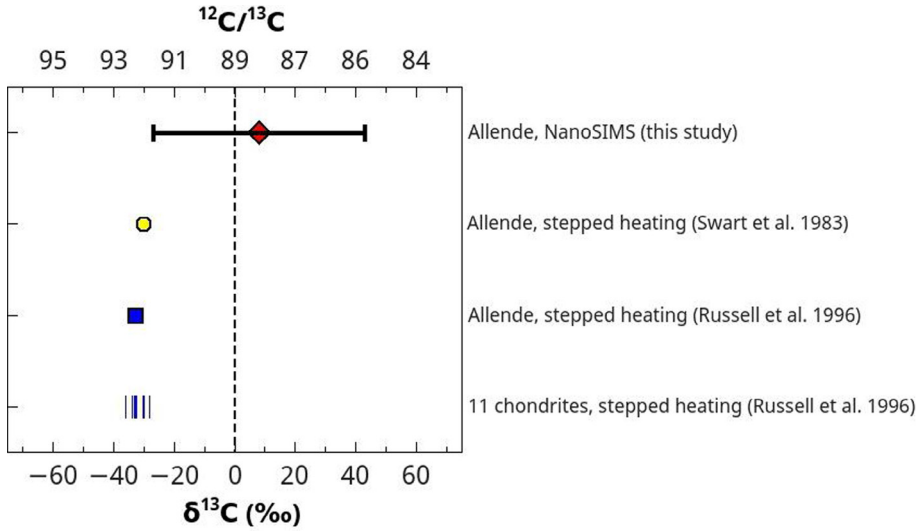

Fig. 4. Bulk measurement of $\delta^{13}C$ compared to previous studies. Data points from previous studies are the average $\delta^{13}C$ detected over the course of stepped heating of less than 100 μg of nanodiamond-containing acid residue per sample (Russell et al., 1996), and 34–68 ng per step (Swart et al., 1983). The minimum $\delta^{13}C$ (most extreme anomaly) is a few per mil farther from terrestrial in each case. The error bars for the data point from Allende, this study, are $\pm 1\sigma$. Swart et al. (1983) do not report errors. Errors for Allende by Russell et al. (1996) are smaller than the size of the symbol. Errors are 0.1 to a few per mil for the range of 10 chondrites by Russell et al. (1996).

It is much less likely for several consecutive anomalies to occur by chance compared to the likelihood of just one occurring. Therefore, the Allende outliers are much more significant than those in the standard materials.

3.3. Broadening of ratio distributions

If a number of isotopically anomalous grains are scattered throughout our measurements, this will lead to some measurements that are shifted towards the anomalous value, relative to a Gaussian distribution. Any individual measurement may be well within uncertainty of the mean, and the distribution need not be double-peaked. However, the distribution will be broader overall. We quantified how far each of the observed $^{12}C/^{13}C$ mean isotope ratios for a distribution varies from a Gaussian curve due to systematics, B_S, and then calculated how much Gaussian broadening the Allende mean ratios exhibit compared to the standards, B_G.

We used all the data points from a given data set in a single distribution, which minimizes $Err(\sigma)$. On the order of 10^6 nanodiamonds are in each of the three Allende distributions. B_S varies from 0.2 to −1.4% of the experimental standard deviation across our different standards, and from −0.1 to −1.9% across the three meteoritic data sets. That is to say, each of our data sets is a good fit to a Gaussian curve, and the Allende material has the same or less systematic error than our standard materials.

However, the standard deviations of the Allende data sets are greater than those of the standards as a fraction of the mean ratio, in every case except for the carbon paint (Table 2, Fig. 8). This is primarily the result of the effect of different count rates on the analysis of the data. The variation of total C counts per data point is different for each data set, as a result of summing over cycles with different count rates per pixel (Table 2, ^{12}C counts variation). For data sets with lower count rates (e.g., DND), cycles with small numbers of counts may be summed very close to the target of 2917 counts per data point, but for data sets with very high counts per pixel (e.g., CPT), where each pixel adds several thousand counts to the sum, the variation is much greater.

The standard data sets show a linear correlation between the variation in the ^{12}C counts and the Gaussian broadening, albeit a poor one (R^2=0.85 from a regressive linear fit) (Fig. 8). Counts variation is therefore a good explanation for why the DND data sets have the lowest broadening, the GRP intermediate, and CPT the highest. However, the ADM data sets do not follow this trend. Adding them to the linear fit gives $R^2 = 0.37$. ADM 26-1 plots close to the line suggested by the standard data sets, albeit not on it – the trend of Gaussian broadening with variation in counts predicts a higher Gaussian broadening for ADM 26-1. ADM 26-3 and 27-3 are much broader than predicted by their counts variations. Taken by themselves, the 3 ADM data sets suggest the opposite of the expected trend: as variation in counts increases sharply, Gaussian broadening decreases. Therefore, the broadening of the ADM data sets, especially ADM 26-3 and ADM 27-3, is not solely attributable to statistical causes; the best explanation is that multiple isotopic reservoirs contribute to these distributions.

3.4. Silicon-containing materials in the Allende residue

The maximum ratio of ^{28}Si counts to $^{12}C + {}^{13}C$ counts in any data point was 6%. In most cases the silicon signal was less than 1%. Lewis et al. (1989) noted 600 ppm SiC (0.06%) so we do not expect to be sensitive to individual SiC grains with close-to-solar isotopic ratios.

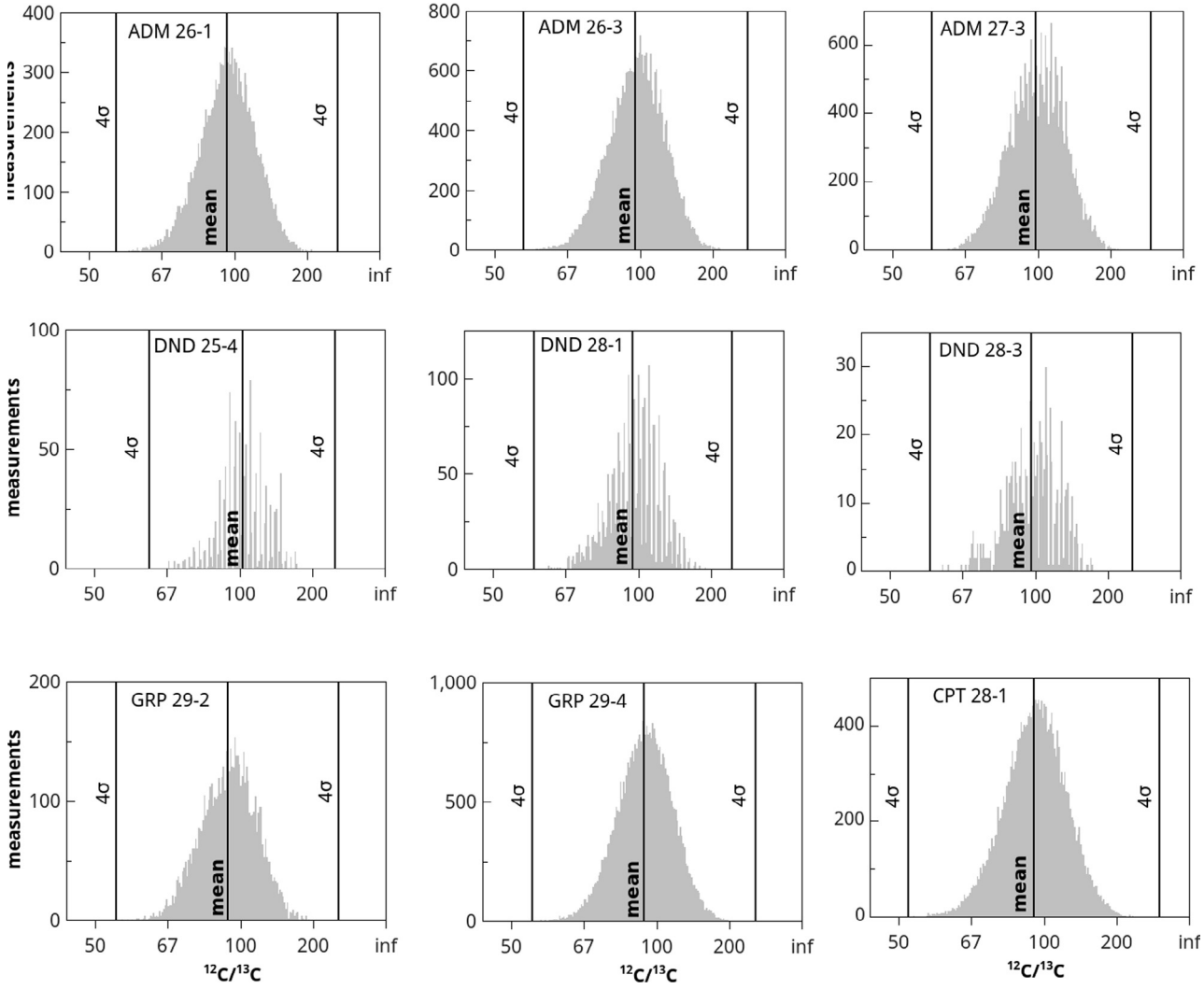

Fig. 5. Histogram of measurements for data sets. The mean and 4σ deviations in each direction are marked. The abscissa is not linearly scaled, rather it is in terms of $^{13}C/^{12}C$. Histograms and deviations are calculated using $^{13}C/^{12}C$, because small errors in ^{13}C create large tails at high $^{12}C/^{13}C$ that do not represent statistically significant outliers. Labels are in $^{12}C/^{13}C$ for ease of reading. The data sets have roughly the same average C counts per data point. The center of the distribution for each data set is at a slightly higher $^{12}C/^{13}C$ ratio than the mean because ratios with higher $^{12}C/^{13}C$ ratios have slightly lower counts on average, a statistical feature inherent to distributions of ratios (Ogliore et al., 2011).

3.5. Detection limits

While direct measurement of isotopically anomalous material is most compelling, it is also informative to consider the isotopic anomalies that were *not* detected, but would have been, if present. It is possible that many different isotopically anomalous populations make up the nanodiamonds. Even limiting our discussion to one solar component and one presolar, isotopically anomalous, component, there remain two variables: the fraction of the measured material that is anomalous, and the magnitude of the anomaly.

For the analyses presented in Section 3.1, the observed bulk ratio would be anomalous if it differed from the solar system ratio by more than 2σ, that is, is less than $^{12}C/^{13}C = 82.1$ or more than 97.2. Fig. 9 illustrates the anomalous fractions that would result in such an observation. Each point on the plot describes a hypothetical aggregate of nanodiamonds made of two components: one "normal" with a solar isotopic ratio, the other anomalous, with a $^{12}C/^{13}C$ ratio R_a, which is plotted on the x-axis, from $^{12}C/^{13}C = 0$ to 150. The anomalous component comprises a fraction f_a of the aggregate, which is plotted on the y-axis from 0 to 100%.

For our bulk ratio measurement presented in Section 3.1, we use Eq. (16) with R_o set to 82.1 (Fig. 9, the solid green line at the left, lower ratio) and 97.2 (the solid green line on the right, higher ratio. The technique in Section 3.1 is sensitive to any anomalous components lying on or above the curves, in the regions marked I and II (a and b). All

Table 2
Statistical data for distributions of isotopic ratio measurements.

Data set	N[a]	CPM[b]	$^{13}C/^{12}C \pm$ SEOM[c]	$\sigma \pm$ Err (σ)	Gaussian broadening (%)[d]	^{12}C counts variation[e]
ADM 26-1	14,852	3009	0.01053 ± 0.00002	0.00191 ± 0.00001	0.6	342
ADM 26-3	30,879	3447	0.01032 ± 0.00001	0.00193 ± 0.00001	1.2	84
ADM 27-3	26,372	2918	0.01015 ± 0.00001	0.00193 ± 0.00001	1.5	49
DND 25-4	1062	2917	0.00983 ± 0.00005	0.00160 ± 0.00003	−1.21	12
DND 28-1	2572	2918	0.01039 ± 0.00003	0.00170 ± 0.00002	−1.11	20
DND 28-3	706	2919	0.01029 ± 0.00007	0.00175 ± 0.00005	−0.54	24
GRP 29-2	6448	3118	0.01090 ± 0.00002	0.00191 ± 0.00002	0.04	233
GRP 29-4	38,400	3123	0.01089 ± 0.00001	0.00192 ± 0.00001	0.16	277
CPT 28-1	23,159	2430	0.01070 ± 0.00001	0.00216 ± 0.00001	2.67	418

[a] N is the number of measurements (data points) for the data set.
[b] Similar mean C counts per measurement (CPM) are achieved by summing multiple cycles for the same pixel into a single measurement.
[c] Ratios are not normalized. SEOM stands for the standard error of the mean, which is the uncertainty in the mean ratio.
[d] Gaussian broadening, B_G, is the difference between σ for that data set as a fraction of the mean, and the mean value of the fractional standard deviation for all the standard data sets.
[e] The standard deviation of CPM, the counts per measurement, for this data set.

Table 3
Outlier data points.[a]

Sample	Depth-row-column			Outlier magnitude ($\times\sigma$)	$^{12}C/^{13}C$ (normalized)		^{12}C	^{13}C	^{28}Si	^{16}O
ADM 26-1	10	8	3	4.065	50	$^{+9}_{-7}$	2406	44	3	207
	27	11	10	4.265	49	$^{+9}_{-6}$	2464	46	6	199
	30	12	11	4.183	49	$^{+8}_{-6}$	2971	55	4	171
ADM 26-3	62	13	4	4.020	50	$^{+9}_{-6}$	2764	50	2	233
	63	13	4	4.349	49	$^{+8}_{-6}$	2777	52	3	243
CPT 28-1	0	2	4	4.095	47	$^{+9}_{-6}$	2303	45	0	122
	31	11	5	4.388	45	$^{+9}_{-6}$	2082	42	0	102
	34	7	13	4.282	46	$^{+9}_{-6}$	2106	42	0	115
	51	0	3	4.182	46	$^{+9}_{-6}$	2129	42	0	82
GRP 29-4	131	14	9	4.006	49	$^{+8}_{-6}$	2903	54	1	77
	142	14	8	4.675	46	$^{+7}_{-6}$	2866	57	0	75
	144	0	13	4.115	48	$^{+8}_{-6}$	2605	49	0	65

[a] Each outlier samples from approximately 1000 nanodiamonds.

anomalous components lying in these regions are counterindicated by our results in Section 3.1 for aggregates of 4×10^6 nanodiamonds.

For analyses presented in Section 3.2, a 5σ outlier for data set ADM 26-1, similar to the other ADM data sets, would have a ratio of $^{12}C/^{13}C = 45.5$, if isotopically heavy, or $^{12}C/^{13}C = 2044.1$, if isotopically light. If the composition of the material in the measurement were two-part, one having a solar system C-isotope ratio, the other composition would have to make up a minimum 1% of the estimated 8×10^5 carbon atoms sputtered by the beam in order to produce a detectable outlier. Therefore, we can rule out the presence of pure ^{13}C clusters larger than 10^4 atoms, and rule out clusters larger than 8×10^5 carbon atoms with a ratio of 45. Fig. 9 presents the detection limit for this method, with the curve described using Eq. (16) and, setting the observed ratio R_o to 45.5, our limit for a 5σ detection. Similar to the bulk ratio, any combination of anomalous

ratio and fraction lying above the dashed line in region I is ruled out by non-detection, in this case for an aggregate of 1000 nanodiamonds partially sampled, 8×10^5 atoms of carbonaceous material sputtered through, or 2917 detected carbon atoms. We do not plot the curve for $^{12}C/^{13}C = 2044.1$ as it is at very high $^{12}C/^{13}C$ ratio.

4. DISCUSSION

4.1. $^{12}C/^{13}C$ Ratio of the nanodiamond residues

Our bulk measurement in Section 3.1 confirms that the nanodiamond carbon is terrestrial in composition down to 8×10^9 carbon atoms of material, compared to a minimum of 10^{15} carbon atoms in stepped heating measurements. The isotopic composition of the roughly 4×10^6 nanodiamonds represented by this number of carbon atoms is $\delta^{13}C = 8 \pm 35‰$. Our measurement of the Allende DM ratio is about 40‰ heavier in ^{13}C (but with an uncertainty of more than 30‰) than previous measurements by stepped heating (Fig. 4), where bulk Allende acid residue has a $\delta^{13}C$ of $-32.7 \pm 0.1‰$ (Russell et al., 1991) and $-30.4‰$ (Swart et al., 1983).

As represented by the high uncertainty, the precision of our measurement is necessarily low compared to stepped heating experiments, since we are integrating less material and are affected by sample topography and uncertainty in the per mil isotopic ratio of our standard. There may also be sensitivity differences between the terrestrial nanodiamond standard material and the meteoritic acid residue, which could account for the disparity between our measurements and previous studies. On the other hand, the isotopically heavier value we measured could be due to intrinsic isotopic anomalies, as our small sample size allows us much greater sensitivity to isotopic inhomogeneity in small fractions of the sample than earlier measurements.

4.2. Implications of Gaussian broadening

We see significant Gaussian broadening of the Allende distributions compared to that predicted by statistics and comparison to our standards. All our data sets are a good fit to a Gaussian distribution, so this broadening in the Allende data sets is attributable to the distribution being drawn from multiple isotopic ratios. This result does not conflict with bulk studies, in that the mean ratios are still close to solar composition, but it does suggest that a fraction of the nanodiamonds have a non-solar carbon isotopic composition. On the other hand, our detection limits plotted in Fig. 9 for the bulk ratio measurement confirm that the nanodiamonds are not composed primarily of material with a mean carbon isotopic anomaly. In an aggregate of only 4×10^6 nanodiamonds, <20% of the nanodiamonds can have $^{12}C/^{13}C$ below 70 or above 110, <10% can have $^{12}C/^{13}C$ below 60 or greater than 150, and <5% can have $^{12}C/^{13}C$ below 40 or $\gg 150$.

Given a variety of solar masses, supernova models predict a broad range of carbon isotopic ratios, including both ^{13}C-enriched and -depleted material (e.g., Rauscher et al., 2002). Supernova nanodiamonds are therefore good candidates to produce a small Gaussian broadening, because even the presence of a large number of such grains would not require a detectable shift to the mean ratio. The possible fraction and magnitude of the anomaly is further constrained by our bulk ratio and outlier detection limits (see Section 3.5 and Fig. 9). However, we note that it is unlikely that we would have detected any ^{13}C-depleted material, which is expected to be present if supernovae created a number of the nanodiamonds, since our sensitivity to depletions in ^{13}C is limited in low-count scenarios.

4.3. Source of $^{12}C/^{13}C$ outliers

For the data from Section 3.2, each data point samples on average approximately 2900 carbon atoms from aggregates of 4×10^6 atoms of carbonaceous material sputtered from the Allende residue, sampling material from approximately 1000 nanodiamonds in a single layer. The lowest ratio measured was $^{12}C/^{13}C = 49 \pm \sim 7$ (detected three times), about 800‰ isotopically heavier than the mean ratio. The largest anomaly reported in the residues to date is roughly 10‰ isotopically heavier than the bulk acid residue, detected in stepped heating (Swart et al., 1983; Russell et al., 1991; Verchovsky et al., 1998), and has been attributed to a small fraction of non-diamond material, presumed to be disordered C. As noted earlier, the Allende outlier data points are distinct from those in the standards in that each is surrounded by additional data points enriched in ^{13}C compared to the average (Fig. 7). If the Allende outliers are not statistical anomalies, there are several possible explanations.

(1) Presolar silicon carbide grains are expected to be present in the nanodiamonds (Lewis et al., 1989) and could be the source of the ^{13}C-rich outliers we observe. Since they undergo the same size separation procedures as the nanodiamonds, these SiC grains should be on the order of a few nanometers to 10 nm in size. However, we see no evidence for silicon carbide grains in the outliers. Si counts rise for some cycles in some of the outlier depth profiles, but there is no consistent increase in Si counts correlating with the increase in ^{13}C signal. Moreover, the Si concentration is very low, 2–6 counts in each of the outliers. For the purposes of a simple approximation, we assume the useful yield of Si is roughly the same as that for C, 0.5%. Thus 6 silicon atoms, the maximum detected for an outlier, would imply the presence of at most 1200 silicon atoms in the volume sputtered, implying 1200 carbon atoms from the same SiC grain. This is not an unreasonable grain size. If all 1200 hypothesized carbon atoms were ^{13}C – an extreme case – we estimate only 6 would be detected, shifting a solar $^{12}C/^{13}C$ ratio data point to a ratio of about 75, which would not register as an outlier in our Allende data sets. Therefore SiC cannot explain the outliers. In addition, the reported SiC concentration in the Allende residue is estimated at 600 ppm (Lewis et al., 1989). If the outliers are due to SiC contamination, their isotopic compositions would have

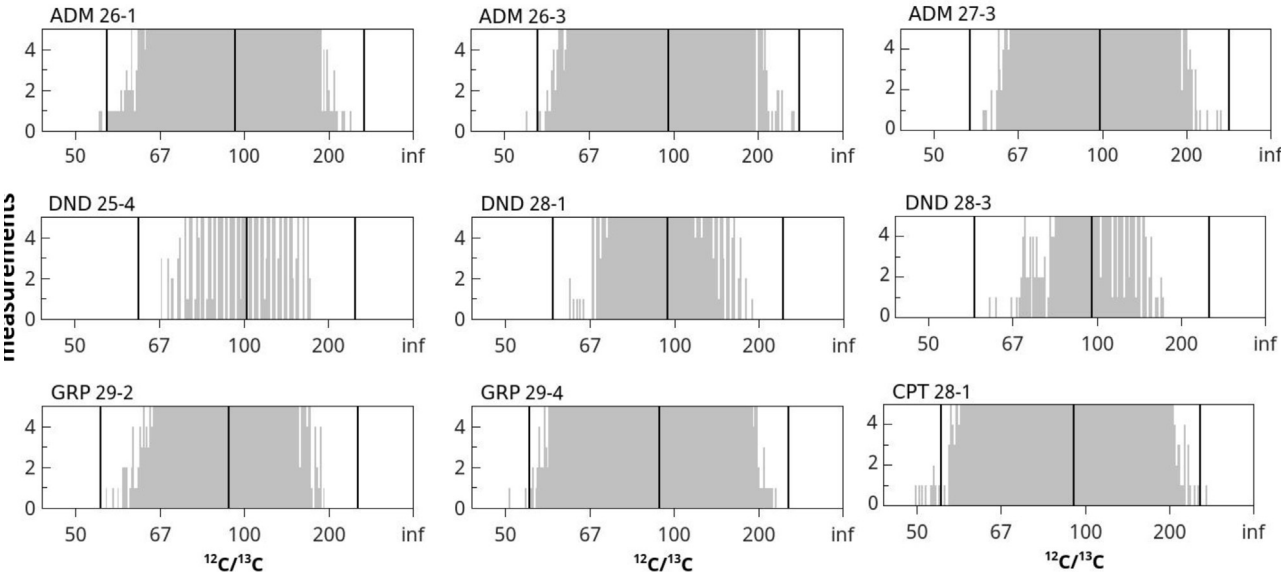

Fig. 6. Vertically stretched view of $^{12}C/^{13}C$ isotopic ratio distributions, highlighting the >4σ outliers in ADM 26-1, ADM 26-3, GRP 29-4, and CPT 28-1. Left to right, the three vertical lines in each image are −4σ, mean, and +4σ in $^{12}C/^{13}C$. All outliers are to the ^{13}C-enriched side.

Table 4
Observed vs. predicted numbers of outliers.

Sample	Measurements	>4σ outliers observed	>4σ outliers expected
ADM	67,312	5	4.3
DND	4340	0	0.3
GRP	44,848	3	2.8
CPT	23,159	4	1.5

to be highly ^{13}C-enriched, similar to SiC AB grains. These grains comprise approximately 5% of the presolar SiC population (Hynes and Gyngard, 2009; Zinner, 2014). Therefore, the detection of 5 SiC AB grains would suggest that there are 100 total presolar SiC grains scattered throughout our meteoritic data sets, a concentration of approximately 25 ppm, given our estimation of 4×10^6 nanodiamonds. If the outliers are caused by SiC AB grains, it is difficult to explain why we do not see an order of magnitude more of them, enough to create a notable peak in the tail of each of our distributions. The fact that we do not see such a secondary peak calls into doubt whether our samples contain 600 ppm SiC, and further confirms that the outliers are not the result of SiC AB grains.

(2) An isotopically anomalous subpopulation of nanodiamonds and/or clumps of disordered sp^2-bonded carbon could be present in the acid residues. For a single anomalous grain to produce an outlier of the magnitude observed, it would be required to be highly enriched in ^{13}C and fill a significant percentage of the analysis area. Nanodiamonds as large as 10 nm in diameter have been reported (Daulton et al., 1996), and their maximum cross-sections would fill about 2% of a 70 nm diameter beam spot. If our spot is actually only 50 nm in diameter, the effect doubles to 4%. Assuming the rest of the material has a $^{12}C/^{13}C$ ratio of 89, a 10 nm presolar grain would be required to have a $^{12}C/^{13}C$ ratio of about 1 for the 2% case, or 4 for the 4% case, in order to produce the isotopic outliers detected with a $^{12}C/^{13}C$ ratio of about 50. This scenario would favor grains from stars with cool bottom processing, including J-stars or novae (Zinner, 2014), but does not rule out other sources, such as born-again AGB stars (Zinner, 2014) and supernovae (Nittler and Hoppe, 2005; Liu et al., 2016). Xe-HL could be implanted into J-star or nova nanodiamond grains in the interstellar medium by a passing supernova shock. However, the presence of a few large presolar nanodiamonds does not explain all of the Xe-HL in the residues, which, in the meteorite Efremovka, is detected in all size fractions (Gilmour et al., 2005).

(3) If more than one presolar grain is present in an outlier data point, smaller anomalies in these grains could produce the outliers observed. In this case we hypothesize presolar nanodiamond material with an average $^{12}C/^{13}C$ ratio of 45. However, the higher the number of presolar grains that are needed to account for an outlier, the more data points must, according to binomial statistics, contain a significant number of these grains. While many data points would contain too few presolar nanodiamonds to register as outliers, the cumulative effect would broaden the distribution and shift the mean ratio. The mean ratio could be balanced by isotopically light material, but broadening of the distribution could not. For a mean presolar nanodiamond $^{12}C/^{13}C$ ratio of 45, as much as 80% of the material in each outlier would need to be composed of presolar nanodiamonds to produce an observed outlier of

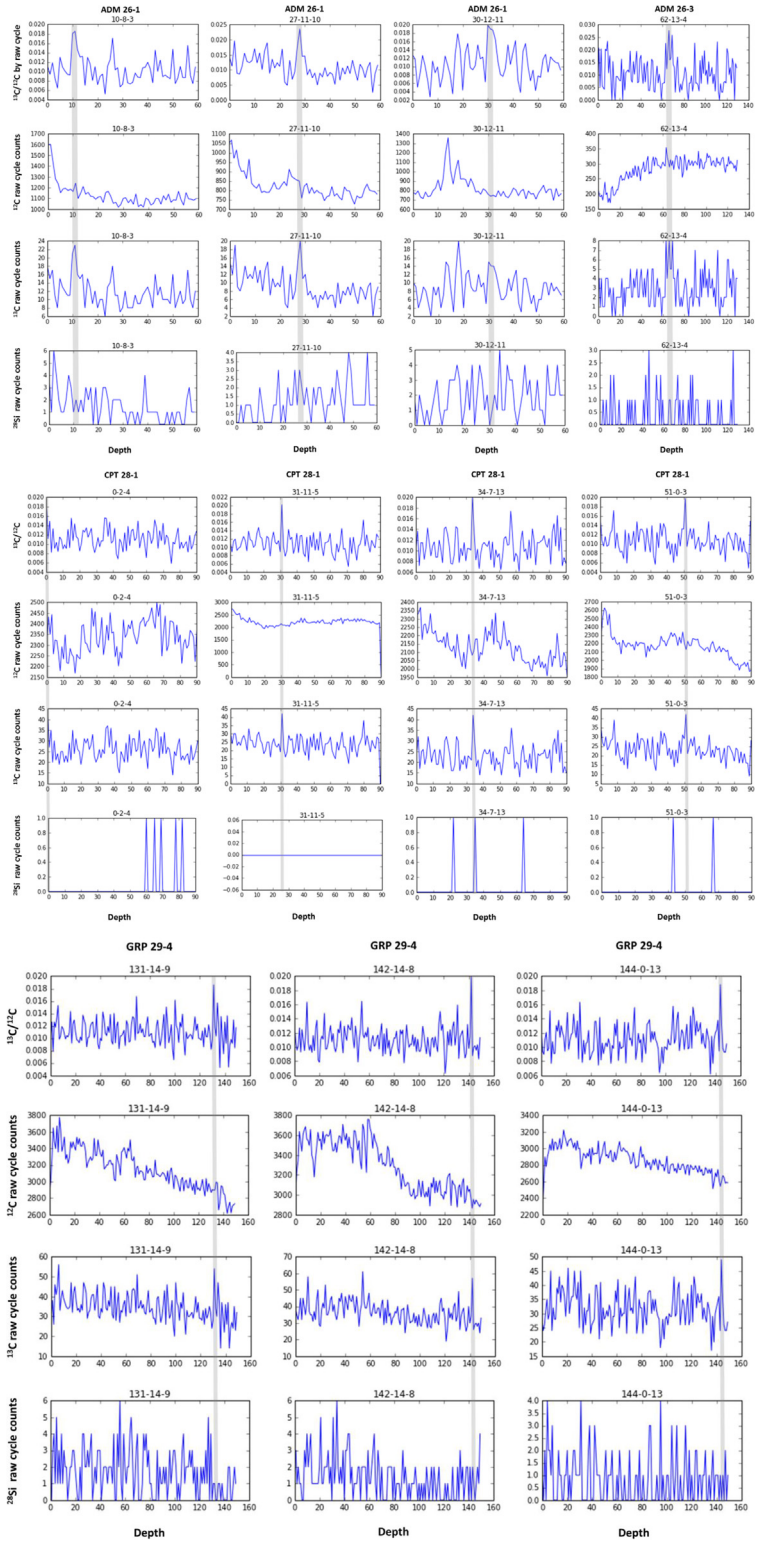

Fig. 7. Depth profiles for 4σ and greater outliers in each Allende and standard material data set. Each profile is labeled *depth-row-column*. Row and column indicate the pixel position in a 16 × 16 image. For Allende data, $^{13}C/^{12}C$ by raw cycle, ^{12}C counts, ^{13}C counts, and ^{28}Si counts are presented. Data points used in the outlier searches and histograms (Figs. 5 and 6) are constructed from the counts of several of the consecutive cycles plotted here as depth. But for each of the depth profiles for standards, each data point was only over 1 cycle, so the counts for a single step in depth here represent the same counts that were used in outlier searches and histograms (Figs. 5 and 6). Ratios are given in $^{13}C/^{12}C$ to avoid low counts in the denominator that would skew the appearance of the profiles. ADM 26-3 row 13 pixel 4 is unique in that data points 62-13-4 and 63-13-4 are consecutive >4σ outliers. Each plot is scaled to fit all the cycle data for that plot.

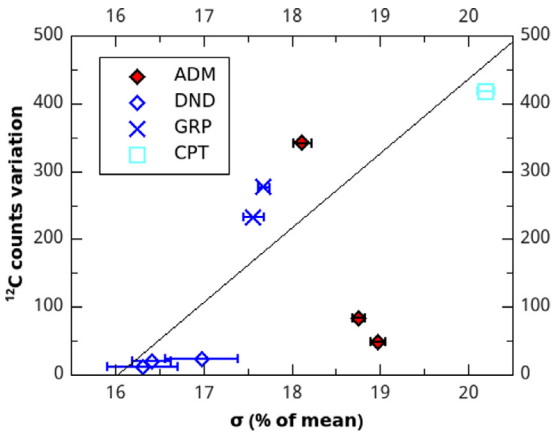

Fig. 8. Variation in ^{12}C counts per data point for each data set plotted versus ^{12}C/^{13}C standard deviations as a percentage of the respective mean values. The various standards show a trend towards broader distributions of ^{12}C/^{13}C ratios for higher variation in ^{12}C counts per data point. The diagonal line is a linear fit to all the data sets except the three from ADM. One meteoritic data set has a ratio distribution slightly narrower than predicted by the linear fit to the standards. The other two meteoritic data sets have ^{12}C/^{13}C ratio distributions several percent broader than can be explained by statistics. The best explanation for the breadth of these data sets is that they are composed of material drawn from multiple isotopic reservoirs.

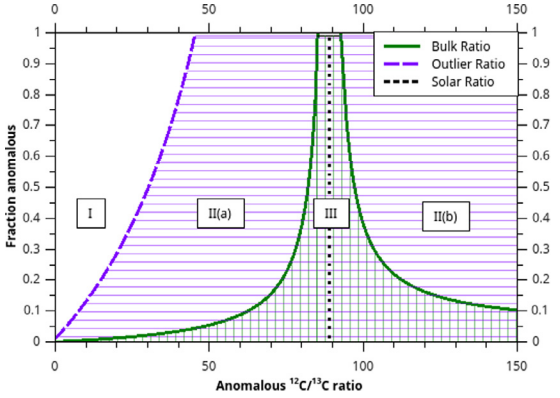

Fig. 9. Detection limits for isotopic anomalies in C for small beam (~70 nm) NanoSIMS measurements of meteoritic nanodiamonds for two sample sizes. Presolar inclusions with anomalous ratios ranging from 0 to 150 are considered, comprising 0–100% of the sample size. Inclusions outside of the vertically lined region (III) are ruled out by our measurements, for aggregates of 4×10^6 nanodiamonds or 8×10^9 atoms of carbonaceous material sputtered through. Presolar inclusions falling in Regions I and II(a and b) would be detected as an anomalous bulk ^{12}C/^{13}C ratio with a greater anomaly than the experimental uncertainty reported in Section 3.1. Inclusions in the horizontally-lined regions (IIa and IIb) are ruled out by our measurements for aggregates of approximately 1000 nanodiamonds, or 8×10^5 atoms of carbonaceous material sputtered through. Presolar inclusions falling in region I would be observed as 5σ or greater outliers using our experimental methodology. A curve for outlier sensitivity to ^{13}C-depleted material, which would lie above ^{12}C/^{13}C = 150 is not shown.

^{12}C/^{13}C = 50.Then, in order for 3 out of the 14,852 (0.02%) of the data points to be outliers for ADM 26-1, and 2 out of 30,879 (0.0065%) for ADM 26-3, the mean percentage of presolar nanodiamonds per data point must be over 15% for ADM 26-1, and over 10% for ADM 26-3. This could be balanced if the remaining material had a mean ratio of 109, for ADM 26-1, and 101, for ADM 26-3. The resulting standard deviation would then be derived from that of the two isotopic sources, which would produce the Gaussian broadening in ratio distributions that we detected. These proportions are similar to the proportions of isotopically light and heavy grains observed in SiC X grains of supernova origin (Zinner, 2014). However, the likelihood of such an ad hoc distribution is not very high.

5. SUMMARY

(1) We have demonstrated that the nanodiamonds and disordered carbon in the Allende DM residues have ^{12}C/^{13}C ratios consistent with solar system values and previous measurements, down to aggregates as small as 10^6 carbon atoms, or 10^3 nanodiamonds.

(2) While our sensitivity rules out large populations of highly anomalous material, a smaller but still significant fraction of the nanodiamonds could carry major isotopic anomalies.

(3) The distributions of the Allende ratios have larger standard deviations than comparable standard data sets, but are still Gaussian in shape. This suggests that multiple isotopic ratios may be represented in the residue, averaging to solar abundances. Presolar nanodiamonds from supernova material, with a range of ^{13}C-enriched and -depleted material, are a good candidate for such a non-solar component, although a fraction of AGB material could also be present together with isotopically light supernovae material.

(4) In addition to broadening over the whole data set, ^{13}C-rich material is observed in several individual aggregates of 10^6 carbon atoms in size, suggesting the presence of a small fraction of ^{13}C-rich nanodiamonds. For SiC, past studies have indicated J-type carbon stars, born-again AGB stars, or nova grains as sources for such grains (Zinner, 2014), but more recent work suggests that they could also come from supernovae (Nittler and Hoppe, 2005; Liu et al., 2016).

(5) The results, taken together, support the conclusion suggested by the presence of Xe-HL, that some of the nanodiamonds are presolar. The broadening of the distributions of ratios in the Allende data compared to standards, as well as data points with ^{13}C-rich ratios, suggest the presence of supernova nanodiamonds. Nanodiamonds from AGB stars or other sources could also be present and could account for both the outliers and the distribution broadening,

but only in conjunction with supernova material to balance out the close-to-solar average $^{12}C/^{13}C$ ratio and to serve as carriers of the Xe-HL.

(6) Additional experimental and statistical work on smaller aggregates is necessary to confirm and expand on these results. Ideally, this would be carried out with a stable, <50 nm-diameter NanoSIMS beam and control software modified to allow for serialized long measurements, or with atom-probe tomography, which can analyze nanodiamonds individually.

ACKNOWLEDGEMENTS

The authors express particular gratitude to inspiration and guidance from Tom Bernatowicz, and acknowledge his contribution of the idea of using a minimized NanoSIMS beam and a statistical approach to detecting isotopic anomalies in presolar nanodiamonds. The authors gratefully acknowledge Frank Podosek for his helpful assistance and contribution to an abstract on an earlier iteration of this work. The authors gratefully acknowledge Larry Nittler and his L'Image software, and Ryan Ogliore for helpful discussions. The authors gratefully acknowledge associate editor Peter Hoppe, reviewer Thomas Stephan, and an anonymous reviewer, each for insightful suggestions that improved the manuscript. Funding: This work was supported by the National Aeronautics and Space Administration [grant numbers NNX14AP15H, NNX16AD26G].

REFERENCES

Amari S., Zinner E. and Gallino R. (2014) Presolar graphite from the Murchison meteorite: an isotopic study. *Geochim. Cosmochim. Acta* **133**, 479–522.

Bernatowicz T. J., Gibbons P. C. and Lewis R. S. (1990) Electron energy loss spectrometry of interstellar diamonds. *Astrophys. J.* **359**, 246–255.

Clayton D. D. (1989) Origin of heavy xenon in meteoritic diamonds. *Astrophys. J.* **340**, 613–619.

Clayton D. D., Meyer B. S., Sanderson C. I., Russell S. S. and Pillinger C. T. (1995) Carbon and nitrogen isotopes in Type II supernova diamonds. *Astrophys. J.* **447**, 894–905.

Coplen T. B., Böhlke J. K., De Bièvre P., Ding T., Holden N. E., Hopple J. A., Krouse H. R., Lamberty A., Peiser H. S. and Révész K., et al. (2002) Isotope-abundance variations of selected elements (IUPAC Technical Report). *Pure Appl. Chem.* **74**, 1987–2017, others.

Dai Z. R., Bradley J. P., Joswiak D. J., Brownlee D. E., Hill H. G. M. and Genge M. J. (2002) Possible *in situ* formation of meteoritic nanodiamonds in the early Solar System. *Nature* **418**, 157–159.

Daulton T. L., Eisenhour D. D., Bernatowicz T. J., Lewis R. S. and Buseck P. R. (1996) Genesis of presolar diamonds: comparative high-resolution transmission electron microscopy study of meteoritic and terrestrial nano-diamonds. *Geochim. Cosmochim. Acta* **60**, 4853–4872.

Gilmour J. D., Verchovsky A. B., Fisenko A. V., Holland G. and Turner G. (2005) Xenon isotopes in size separated nanodiamonds from Efremovka: $^{129}Xe^{*}$, Xe-P3, and Xe-P6. *Geochim. Cosmochim. Acta* **69**, 4133–4148.

Greiner N. R., Phillips D. S., Johnson J. D. and Volk F. (1988) Diamonds in detonation soot. *Nature* **333**, 440–442.

Hayya J., Armstrong D. and Gressis N. (1975) A note on the ratio of two normally distributed variables. *Manage. Sci.* **21**, 1338–1341.

Heck P. R., Stadermann F. J., Isheim D., Auciello O., Daulton T. L., Davis A. M., Elam J. W., Floss C., Hiller J., Larson D. J., Lewis J. B., Mane A., Pellin M. J., Savina M. R., Seidman D. N. and Stephan T. (2014) Atom-probe analyses of nanodiamonds from Allende. *Meteorit. Planet Sci.* **49**, 453–467.

Hillion F., Daigne B., Girard F. and Slodzian G. (1995) The CAMECA "NANOSIMS 50" experimental results. *SIMS* **X**, 979–982.

Hoppe P., Leitner J. and Kodolányi J. (2015) New constraints on the abundances of silicate and oxide stardust from supernovae in the Acfer 094 meteorite. *Astrophys. J. Lett.* **808**, L9 (6 pp).

Huss G. R. (2005) Meteoritic nanodiamonds: messengers from the stars. *Elements* **1**, 97–100.

Huss G. R. and Lewis R. S. (1994a) Noble gases in presolar diamonds I: Three distinct components and their implications for diamond origins. *Meteoritics* **29**, 791–810.

Huss G. R. and Lewis R. S. (1994b) Noble gases in presolar diamonds II: Component abundances reflect thermal processing. *Meteoritics* **29**, 811–829.

Huss G. R. and Lewis R. S. (1995) Presolar diamond, SiC, and graphite in primitive chondrites: abundances as a function of meteorite class and petrologic type. *Geochim. Cosmochim. Acta* **59**, 115–160.

Huss G. R., Ott U. and Koscheev A. P. (2008) Noble gases in presolar diamonds III: Implications of ion implantation experiments with synthetic nanodiamonds. *Meteorit. Planet. Sci.* **43**, 1811–1826.

Hynes, K. M., Gyngard, F., 2009. The presolar grains database: <http://presolar.wustl.edu/~pgd>. *Lunar and Planet. Sci. XL.* Lunar Planet. Inst., Houston. #1198 (abstr.).

Isheim D., Stadermann F. J., Lewis J. B., Floss C., Daulton T. L., Davis A. M., Heck P. R., Pellin M. J., Savina M. R., Seidman D. N. and Stephan T. (2013) Combining atom-probe tomography and focused-ion beam microscopy to study individual presolar meteoritic nanodiamond particles. *Microsc. Microanal.* **19**(Suppl 2), 974–975 (abstr.).

Lewis J. B., Isheim D., Floss C. and Seidman D. N. (2015) $^{12}C/^{13}C$-ratio determination in nanodiamonds by atom-probe tomography. *Ultramicroscopy* **159**, 248–254.

Lewis J. B., Isheim D., Floss C., Daulton T. L. and Seidman D. N. (2016) Analysis of Allende nanodiamond residue by correlated transmission electron microscopy and atom-probe tomography. *Lunar Planet. Sci.* **XLVII**, #2248 (abstr.).

Lewis R. S., Ming T., Wacker J. F., Anders E. and Steel E. (1987) Interstellar diamonds in meteorites. *Nature* **326**, 160–162.

Lewis R. S., Anders E. and Draine B. T. (1989) Properties, detectability and origin of interstellar diamonds in meteorites. *Nature* **339**, 117–121.

Liu N., Nittler L. R., Alexander C. M. O'. D., Wang J., Pignatari M., José J. and Nguyen A. (2016) Stellar origins of extremely ^{13}C- and ^{15}N-enriched presolar SiC grains: Novae or supernovae? *Astrophys. J.* **820**, 140 (14 pp).

Maas R., Loss R. D., Rosman K. J. R., De Laeter J. R., Lewis R. S., Huss G. R. and Lugmair G. W. (2001) Isotope anomalies in tellurium and palladium from Allende nanodiamonds. *Meteorit. Planet. Sci.* **36**, 849–858.

Marty B., Chaussidon M., Wiens R. C., Jurewicz A. J. G. and Burnett D. S. (2011) A ^{15}N-poor isotopic composition for the solar system as shown by Genesis solar wind samples. *Science* **332**, 1533–1536.

Nittler L. R. and Hoppe P. (2005) Are presolar silicon carbide grains from novae actually from supernovae? *Astrophys. J. Lett.* **631**, L89–L92.

Nuth J. A. and Allen J. E. (1992) Supernovae as sources of interstellar diamonds. *Astrophys. Space Sci.* **196**, 117–123.

Ogliore R. C., Huss G. R. and Nagashima K. (2011) Ratio estimation in SIMS analysis. *Nucl. Instr. Meth. Phys. Res. B* **269**, 1910–1918.

Pravdivtseva O., Shatoff E. A., Meshik A. and Stroud R. M. (2016) Separation of Allende nanodiamonds by electrophoresis. *Lunar Planet. Sci.* **XLVII**, #2996 (abstr.).

Rauscher T., Heger A., Hoffman R. D. and Woosley S. E. (2002) Nucleosynthesis in massive stars with improved nuclear and stellar physics. *Astrophys. J.* **576**, 323–348.

Richter S., Ott U. and Begemann F. (1998) Tellurium in pre-solar diamonds as an indicator for rapid separation of supernova ejecta. *Nature* **391**, 261–263.

Russell S. S., Arden J. W. and Pillinger C. T. (1991) Evidence for multiple sources of diamond from primitive chondrites. *Science* **254**, 1188–1191.

Russell S. S., Arden J. W. and Pillinger C. T. (1996) A carbon and nitrogen isotope study of diamond from primitive chondrites. *Meteorit. Planet. Sci.* **31**, 343–355.

Schelhaas N., Ott U. and Begemann F. (1990) Trapped noble gases in unequilibrated ordinary chondrites. *Geochim. Cosmochim. Acta* **54**, 2869–2882.

Shatoff E. A., Meshik A. P. and Pravdivtseva O. V. (2015) Electrophoresis of Allende nanodiamonds in colloidal solution. *Lunar Planet. Sci.* **XLVI**, #2688 (abstr.).

Shigemitsu T., Matsumoto G. and Tsukahara S. (1979) Electrical properties of glassy-carbon electrodes. *Med. Biol. Eng. Comput.* **17**, 465–470.

Slodzian G., Hillion F., Stadermann F. J. and Zinner E. (2004) QSA influences on isotopic ratio measurements. *Appl. Surf. Sci.* **231–232**, 874–877.

Stroud R. M., Chisholm M. F., Heck P. R., Alexander C. M. O'D. and Nittler L. R. (2011) Supernova shock-wave-induced co-formation of glassy carbon and nanodiamond. *Astrophys. J. Lett.* **738**, L27 (5 pp).

Stroud R. M., Pravdivtseva O. V., Meshik A. P. and Shatoff E. A. (2016) Aberration-corrected STEM analysis of electrophoresis separates of Allende nanodiamond. *Lunar Planet. Sci.* **XLVII**, #2311(abstr.).

Swart P. K., Grady M. M., Pillinger C. T., Lewis R. S. and Anders E. (1983) Interstellar carbon in meteorites. *Science* **220**, 406–410.

Taylor, J. R., 1997. *An introduction to error analysis*, second ed. University Science Books, California, U.S.A. (first ed. 1982).

Tielens, A. G. G. M., 1990. Carbon stardust: From soot to diamonds. In *Carbon in the Galaxy: Studies from Earth and Space*, pp. 59–111.

Verchovsky A. B., Fisenko A. V., Semjonova L. F., Wright I. P., Lee M. R. and Pillinger C. T. (1998) C, N, and noble gas isotopes in grain size separates of presolar diamonds from Efremovka. *Science* **281**, 1165–1168.

Verchovsky A. B., Fisenko A. V., Semjonova L. F., Bridges J., Lee M. R. and Wright I. P. (2006) Nanodiamonds from AGB stars: a new type of presolar grain in meteorites. *Astrophys. J.* **651**, 481–490.

Yastrebov S. and Smith R. (2009) Nanodiamonds enveloped in glassy carbon shells and the origin of the 2175 Å optical extinction feature. *Astrophys. J.* **697**, 1822–1826.

Ziegler J. F., Ziegler M. D. and Biersack J. P. (2010) SRIM – The stopping and range of ions in matter (2010). *Nucl. Instr. Meth. Phys. Res. B* **268**, 1818–1823.

Zinner, E., 2014. Presolar Grains. In Treatise on Geochemistry (eds. H. D. Holland, K. K. Turekian; vol. ed. A. M. Davis). Elsevier Ltd., Oxford, second ed.. **vol. 1.4**, pp. 181–213.

Associate editor: Anders Meibom